

Hole-Transporting Small Molecules Based on Thiophene Cores for High Efficiency Perovskite Solar Cells

Hairong Li,^[a] Kunwu Fu,^[a] Pablo P. Boix,^[a] Lydia H. Wong,^[a] Anders Hagfeldt,^[b] Michael Grätzel,^[c] Subodh G. Mhaisalkar,^{*,[a]} and Andrew C. Grimsdale^{*,[a]}

Two new electron-rich molecules, 2,3,4,5-tetra[4,4'-bis(methoxyphenyl)aminophen-4"-yl]-thiophene (H111) and 4,4',5,5'-tetra[4,4'-bis(methoxyphenyl)aminophen-4"-yl]-2,2'-bithiophene (H112), which contain thiophene cores with arylamine side groups, are reported. When used as the hole-transporting material (HTM) in perovskite-based solar cell devices, power conversion efficiencies of up to 15.4% under AM 1.5G solar simula-

tion were obtained. This is the highest efficiency achieved with HTMs not composed of 2,2',7,7'-tetrakis(*N,N'*-di-*p*-methoxyphenylamine)-9,9'-spirobifluorene (spiro-OMeTAD) and its isomers. Both HTMs, especially H111, have great potential to replace expensive spiro-OMeTAD given their much simpler and less expensive syntheses.

Introduction

Following the initial development of mesoscopic dye-sensitized solar cells (DSSCs) by Grätzel and O'Regan in 1991,^[1] it has become possible to achieve standard power conversion efficiencies (PCEs) of > 10% in devices that use liquid electrolytes; the highest efficiency achieved so far under AM 1.5G solar simulation is 13.0%.^[2] However, inherent problems, such as leakage, instability, and the corrosive nature of the redox electrolyte, have so far hindered the large-scale entry of DSSCs into the commercial market. As a result, great efforts are being made to optimize solid hole-transporting materials (HTMs) for such devices. Although inorganic HTMs, such as CuI,^[3] CsSnI₃,^[4] and CuSCN,^[5] have received much attention, to date, most device characterization and optimization work has centered on the most extensively studied HTM: 2,2',7,7'-tetrakis(*N,N'*-di-*p*-methoxyphenylamine)-9,9'-spirobifluorene (spiro-OMeTAD; Figure 1).^[6] However, none of the PCE values for all-solid DSSCs have been able to surpass those of conventional DSSCs, until the emergence of lead-based perovskite-sensitized solar cells,

in which the organic or organometallic dye is replaced by a nanocrystalline lead-based inorganic semiconductor. This relatively old family of materials, which can be made at low cost, has recently proven to exhibit outstanding performance and has rapidly attracted much interest in the photovoltaic community since late 2011.^[6k,7]

Although spiro-OMeTAD and its isomers continue to be the best performing HTMs,^[8] several classical semiconducting polymers, which have been much studied in organic photovoltaic devices, have also been investigated recently as HTMs, including poly-3-hexyl thiophene (P3HT), poly[2,6-[4,4-bis-(2-ethylhexyl)-4*H*-cyclopenta[2,1-*b*;3,4-*b'*]dithiophene]-*alt*-4,7(2,1,3-benzothiadiazole)] (PCPDTBT), poly[*N*-9'-heptadecan-2,7-carbazole-*alt*-5,5'-(4',7'-di-2-thienyl-2',1',3'-benzothiadiazole)] (PCDTBT), and poly[bis(4-phenyl)(2,4,6-trimethylphenyl)amine] (PTAA).^[7f] Except for PTAA, these materials have, for as yet unknown reasons, displayed inferior performance to that of spiro-OMeTAD, with no inherent cost advantage over spiro-OMeTAD, and may indeed suffer problems of batch to batch inconsistency. Recently, a number of small-molecule HTMs, such as simple arylamines^[9] and pyrene arylamines,^[10] have been reported; the latter have shown impressive performance.

Our group previously reported a small molecule that incorporated a heterocyclic 3,4-ethylenedioxythiophene (EDOT)^[11] core (H101), with a very promising PCE of 13.2% when adopted as the HTM in perovskite solar cells (Figure 1). To address some potential issues with H101 (see below), we have developed two new molecules and investigated their performance as the HTM in CH₃NH₃PbI₃ perovskite solar cells, in comparison with reference devices using spiro-OMeTAD.


Results and Discussion

The chemical structures of the two molecules, H111 and H112, are shown in Figure 1. H111 is derived from H101 by replacing

[a] Dr. H. Li, K. Fu, Dr. P. P. Boix, Prof. L. H. Wong, Prof. S. G. Mhaisalkar, Prof. A. C. Grimsdale
Energy Research Institute @ NTU (ERI@N)
School of Materials Science and Engineering
Nanyang Technological University
Nanyang Avenue, Singapore 637553
E-mail: Subodh@ntu.edu.sg
acgrimsdale@ntu.edu.sg

[b] Prof. A. Hagfeldt
Department of Chemistry—Ångström
Uppsala University, Box 523, 75120 Uppsala (Sweden)

[c] Prof. M. Grätzel
Laboratory for Photonics and Interfaces
Institute of Chemical Sciences and Engineering
School of Basic Sciences
Ecole Polytechnique Fédérale de Lausanne
1015 Lausanne (Switzerland)

 Supporting Information for this article is available on the WWW under <http://dx.doi.org/10.1002/cssc.201402587>.

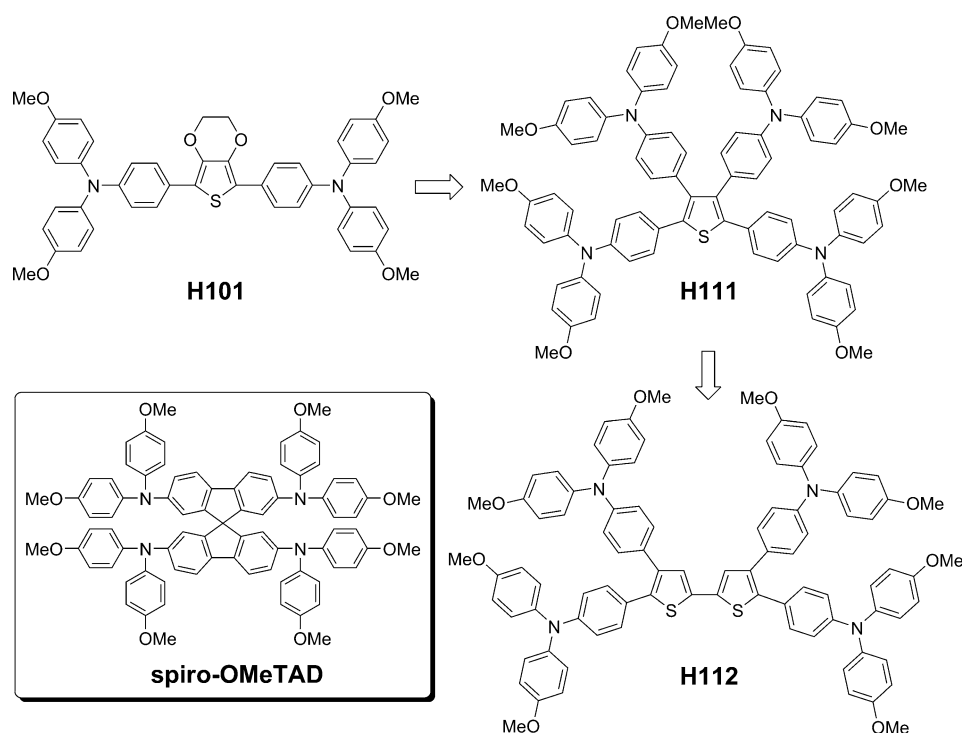
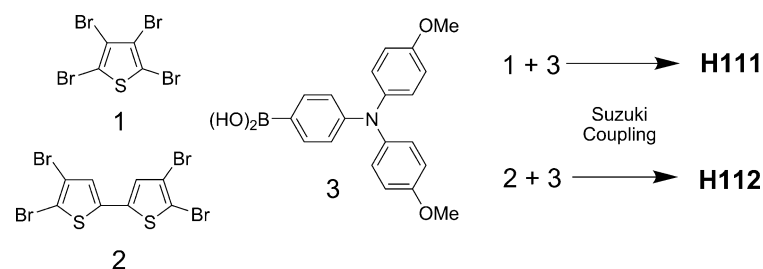


Figure 1. Chemical structures of spiro-OMeTAD, H101 [2,5-bis(4,4'-bis(methoxyphenyl)aminophen-4''-yl)-3,4-ethylenedioxythiophene], 2,3,4,5-tetra[4,4'-bis(methoxyphenyl)aminophen-4''-yl]-thiophene (H111), and 4,4',5,5'-tetra[4,4'-bis(methoxyphenyl)aminophen-4''-yl]-2,2'-bithiophene (H112).

the ethylenedioxy group with two more arylamine units, whereas H112 has a more extended backbone than that of H111. The synthesis of H111 and H112 is very straightforward with good yields (Scheme 1). Tetrabromothiophene (**1**) is commercially available and 4,4',5,5'-tetrabromo-2,2'-bithiophene (**2**) can be synthesized from 2,3-dibromothiophene in 90% yield.^[12] Both precursors are air stable, unlike 2,5-dibromo-EDOT, which is used to make H101 and is rapidly oxidized in air and must be used immediately upon in situ formation or else kept under an inert atmosphere. Both H111 and H112 showed excellent solubility in common solvents, such as chloroform and chlorobenzene (380 g L⁻¹ for H111 and 645 g L⁻¹ for H112 at room temperature), thanks to their abundant methoxy groups and bulky structures, which suppress molecular aggregation.

Differential scanning calorimetry (DSC) measurements (Figure 2 and Table 1) show that H111 has a glass transition temperature (T_g) of 100 °C. This value is significantly higher



Scheme 1. Starting materials and synthetic routes to H111 and H112.

than that of our previously reported H101 ($T_g = 73$ °C^[11]) because replacing the ethylenedioxy group in H101 with two triarylamine in H111 increases the molecular size, leading to a higher value of T_g . By further increasing the length and conjugation of the backbone and reducing steric hindrance among the triarylamine groups in H112, the T_g is further raised to 120 °C, which is comparable with that of spiro-OMeTAD ($T_g = 125$ °C^[13]). The higher T_g values of both new HTMs, relative to H101, may not necessarily improve their photophysical stability at normal operational temperatures, but should at least guarantee their mechanical robustness. The absorption spectra (Figure 2 and Table 1) indicate that H111 starts to absorb light (λ_{onset}) from $\lambda = 446$ nm, which is 27 nm redshifted relative to that of spiro-

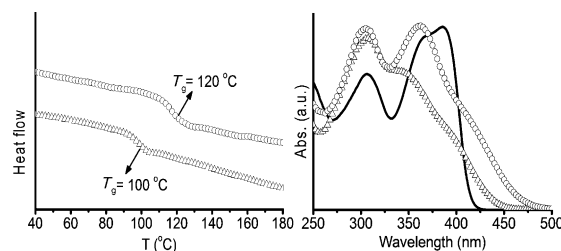


Figure 2. Left: DSC results for H111 (Δ) and H112 (\circ). Right: Absorption spectra of H111 (Δ), H112 (\circ), and spiro-OMeTAD (—).

OMeTAD. The λ_{onset} value of H112 is 477 nm, which is 31 nm redshifted from that of H111 (58 nm redshifted from that of spiro-OMeTAD); this is attributed to the more extended conjugation of the backbone. Cyclic voltammetry (CV) measurements (Figure 3) indicate that the HOMO levels of H111 and H112 are -5.31 and -5.29 eV, respectively. Both are 80–100 meV deeper than that of spiro-OMeTAD (-5.21 eV). The optical and electrochemical data in Table 1 also indicate that the effect of extending the conjugation from H111 to H112 seems to affect the LUMO more the HOMO. Both new HTMs have significantly reduced HOMO levels than that of H101 (-5.16 eV), which not only increases their electrochemical stability, but also reduces the fundamental energy loss (loss-in-potential) by reducing the energy offset required for hole extraction from perovskite to HTM.^[14] In principle, the open-circuit voltage (V_{oc}) of a conventional solid-state DSSC is determined by the differ-

Table 1. Thermal, optical, and electrochemical properties of H111, H112, spiro-OMeTAD, and H101.					
HTM	T_g [°C]	λ_{onset} [nm]	$E_g^{[a]}$ [eV]	HOMO [eV]	LUMO ^[b] [eV]
H111	100	446	2.78	−5.31	−2.53
H112	120	477	2.60	−5.29	−2.69
H101	73	460	2.70	−5.16	−2.46
spiro-OMeTAD	125	419	2.96	−5.21	−2.25

[a] Optical band gap (E_g) obtained from the onset value of absorption (λ_{onset}). [b] LUMO calculated by $\text{LUMO} = \text{HOMO} + E_g$.

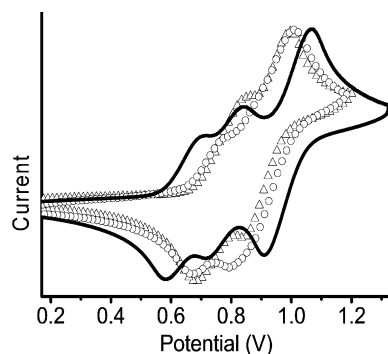


Figure 3. CV spectra of H111 (Δ), H112 (\circ), and spiro-OMeTAD (—).

ence between the quasi-Fermi levels of the electrons in TiO_2 and the holes in the HTM. From the electrochemical experiments, one would expect that the V_{oc} from devices with H111 or H112 as the HTM would be higher than that from devices with spiro-OMeTAD, providing that the interfaces of TiO_2 /perovskite/HTM were properly aligned.

The current–voltage (J – V) characteristics of perovskite solar cells that employ H111, H112, and spiro-OMeTAD as the HTM are shown in Figure 4 and summarized in Table 2. The PCEs of the best performing device with H111, H112, and spiro-OMeTAD as HTM are 15.4, 15.2, and 14.4%, respectively. Our study also showed that the device fabricated without the HTM had a PCE of only around 5%, which confirmed that an HTM must be an integral component of the studied device configuration to obtain a high PCE. Correspondingly, the short-circuit currents (J_{sc}) of the cells are 19.8, 20.0, and 19.9 mA cm^{-2} , respectively. It is clear that the J_{sc} values are all high and almost identical for the three different HTM-based devices. A J_{sc} limit of around 20 mA cm^{-2} has been widely observed in our lab when using $\text{CH}_3\text{NH}_3\text{PbI}_3$ as a perovskite sensitizer following the same device fabrication protocol. As a result, the parameter

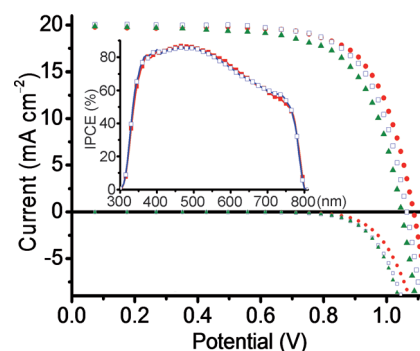


Figure 4. Current–voltage curves of solar cells with H111 (\bullet), H112 (\square), and spiro-OMeTAD (\blacktriangle) as the HTM. Inset: the incident photon to current conversion efficiency (IPCE) spectra of solar cell devices with H111 (\bullet) and H112 (\square) as the HTM.

producing the difference in PCE in these devices is the open-circuit voltage (V_{oc}). From CV studies, it is clear that both new HTMs have almost the same HOMO level, which is about 90 meV deeper than that of spiro-OMeTAD. Therefore, the relatively higher values of V_{oc} for H111 (1.08 V) and H112 (1.07 V), relative to that of spiro-OMeTAD (1.05 V), is to be expected; this enhancement accounts for the marginally higher PCE than that obtained for spiro-OMeTAD. To the best of our knowledge, H111 and H112 are the first reported heterocycle-based materials with PCEs of > 15% in perovskite solar cells, and show by far the highest efficiency achieved with HTMs other than spiro-OMeTAD and its isomers.^[8b]

Electrochemical impedance spectroscopy (EIS) measurements were also performed to characterize both hole transportation in the HTM and the recombination process.^[15] We measured the representative perovskite solar cells with H111, H112, and spiro-OMeTAD as a HTM under illumination. The resulting spectra were fitted by following a previously reported equivalent circuit,^[16] with the introduction of a transmission line for the voltages at which electron transport was visible. The recombination resistance (Figure 5a) presents almost identical behavior for the three analyzed devices, which indicates that the substitution of spiro-OMeTAD by H111 or H112 does not affect the charge loss of the devices. As a result, the differences in V_{oc} follow a similar trend to the HOMO level positions. However, the effect of the variation of these energetic positions on charge generation and injection rates requires further study. The slight variations in the FF can be explained from the series resistance of the different HTM-based cells (R_{HTM}). The R_{HTM} value extracted from the fittings are plotted in Figure 5b. The lower values obtained for both H111- and H112-based solar cells are in excellent agreement with the slightly higher FF values obtained.

For the thermal stability test, we accelerated aging by putting the cells in an oven at 70 °C for 14 days and measured the J – V response every other day. The photovoltaic data are summarized in Figure 6. The results

Table 2. J – V characteristics of photovoltaic measurements for H111, H112, and spiro-OMeTAD as the HTM. ^[a]				
HTM	PCE [%]	J_{sc} [mA cm^{-2}]	V_{oc} [V]	FF
H111	14.9 \pm 0.49 (15.4)	19.66 \pm 0.55 (19.8)	1.07 \pm 0.013 (1.08)	0.71 \pm 0.019 (0.72)
H112	14.7 \pm 0.36 (15.2)	19.70 \pm 0.32 (20.0)	1.07 \pm 0.015 (1.07)	0.70 \pm 0.016 (0.71)
spiro-OMeTAD	14.0 \pm 0.36 (14.4)	19.5 \pm 0.90 (19.9)	1.05 \pm 0.008 (1.05)	0.69 \pm 0.022 (0.69)

[a] Average data with standard deviation were based on five cells in a single batch; the data for the best performing cells are given in parentheses. FF = fill factor.

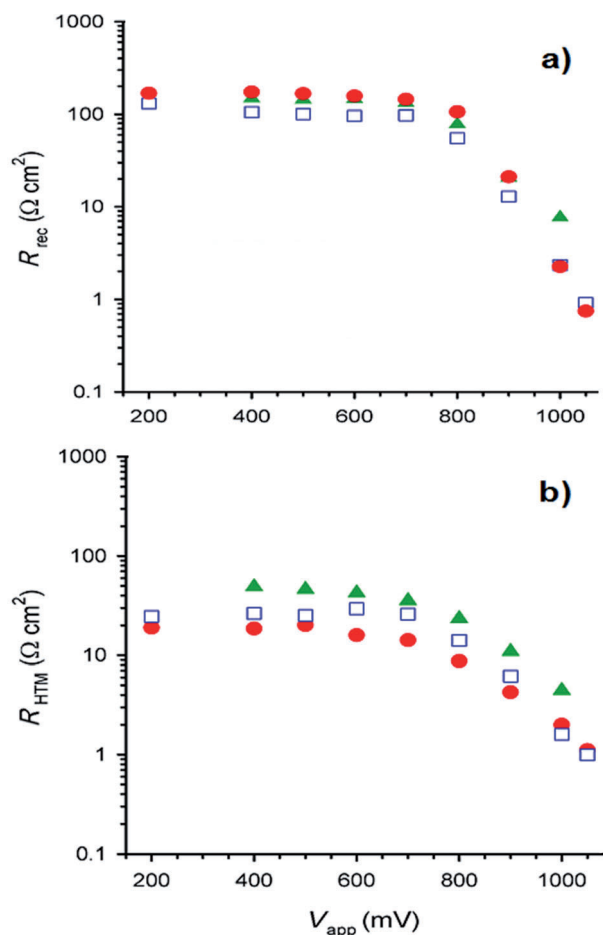


Figure 5. a) Recombination resistance and b) hole-transport resistance extracted from fitting of the EIS results under illumination for perovskite solar cells with H111 (●), H112 (□), and spiro-OMeTAD (▲) as the HTM.

show that all three HTM-based devices have comparable thermal stabilities. The moderate decreases in performance by 16% for both H111- and H112-based devices, and 20% for the spiro-OMeTAD-based devices, are within expectation for unpackaged cells. Although the open-circuit voltage showed negligible changes for H111- and H112-based cells, the decreases

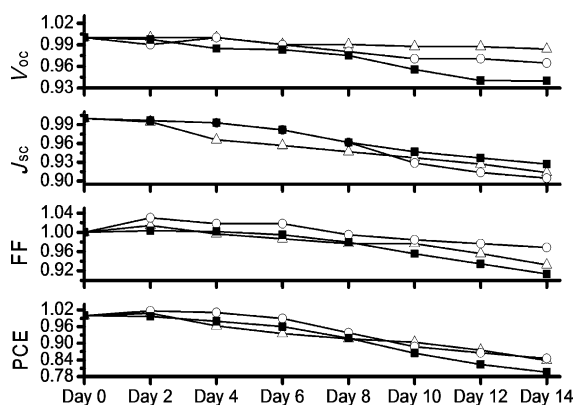


Figure 6. Thermal aging tests for H111- (Δ) and H112-based devices (○), in parallel with the spiro-OMeTAD-based (■) device.

in the short-circuit current and FF were mainly attributed to degradation of the perovskite because gradual color bleaching of the perovskite from the originally dark coffee color was observed over time. We also kept the HTM solutions for spin-coating in the oven and measured the absorption spectra after 14 days without observing noticeable changes. Thus, the limiting factor is the very hydroscopic nature of the perovskite; this causes the efficiency decrease without proper encapsulation.

Conclusions

We reported two new arylamine-type HTMs with tetrasubstituted thiophene and tetrasubstituted bithiophene units as the cores; these produced PCEs that were slightly better than those for devices with conventionally used spiro-OMeTAD. These new materials, H111 and H112, have the following advantages over our previously reported EDOT-based HTM (H101): First, the synthesis of the new HTMs are equally simple, but use cheaper starting materials (thiophene instead of EDOT) and have stable intermediates. Second, the T_g values for the new HTMs are much higher, which should enhance their physical stability within the devices. Third, the HOMO levels of the new HTMs are much deeper than that of H101, which accounts for the higher V_{oc} value of the former. Given the almost identical J_{sc} values for devices with our new materials and spiro-OMeTAD, increasing the V_{oc} seems to be the best strategy to increase PCE. Further understanding of such molecules, and detailed investigations into charge transport in the bulk, as well as functional interfaces, will contribute significantly to improving the efficiency and viability of perovskite solar cells.

Experimental Section

Synthesis of H111

Compound **1** (0.2 g, 0.5 mmol), compound **3** (0.78 g, 2.25 mmol), K_2CO_3 (2 m, 5 mL), and $[Pd^0(PPh_3)_4]$ (60 mg, 0.05 mmol) were dissolved in freshly distilled THF (20 mL). The reaction mixture was then stirred at reflux in the dark for 12 h. The reaction mixture was cooled to RT and poured into water, extracted with CH_2Cl_2 , and washed with water. The organic layer was dried over $MgSO_4$, concentrated, and the residue mixture was purified by column chromatography on silica gel with CH_2Cl_2 /hexane = 4:1 as the eluent to obtain the product as a bright-yellow solid (0.48 g, 74%). 1H NMR (CD_2Cl_2): δ = 7.12–7.01 (m, 12H; PhH), 7.02–6.99 (m, 8H; PhH), 6.88–6.71 (m, 20H; PhH), 6.77–6.73 (m, 8H; PhH), 3.81 (s, 12H; OCH_3), 3.79 ppm (s, 12H; OCH_3); ^{13}C NMR (CD_2Cl_2): δ = 156.6, 156.2, 147.5, 141.4, 140.9, 139.3, 131.9, 130.0, 129.7, 129.4, 128.6, 127.4, 126.7, 125.6, 120.5, 119.5, 115.2, 115.1, 55.89, 55.86 ppm; HRMS (MALDI-TOF): m/z calcd for $C_{84}H_{72}N_4O_8S$: 1296.51; found: 1296.47; elemental analysis calcd (%) for $C_{84}H_{72}N_4O_8S$: C 77.75, H 5.59, N 4.32, S 2.47; found: C 77.62, H 5.61, N 4.24, S 2.55.

Synthesis of H112

H112 was obtained as a yellow solid in 80% yield from **2** and **3** by following the same procedure as that used to make H111. 1H NMR (CD_2Cl_2): δ = 7.43 (dd, J = 6.8 Hz, 4H; PhH), 7.20 (s, 2H; ThH), 7.10–7.08 (m, 8H; PhH), 7.02–6.99 (m, 12H; PhH), 6.92–6.87 (m, 12H;

PhH), 6.81–6.74 (m, 12H; PhH), 3.81 (s, 12H, OCH₃), 3.77 ppm (s, 12H, OCH₃); ¹³C NMR (CD₂Cl₂): δ = 156.7, 156.2, 149.0, 147.8, 144.3, 141.6, 141.3, 140.9, 129.2, 129.1, 127.6, 127.2, 126.6, 126.5, 126.2, 124.1, 120.9, 120.5, 115.1, 115.1, 115.0, 55.9, 55.8 ppm; MS (MALDI-TOF): *m/z* calcd for C₈₈H₇₄N₄O₈S₂: 1378.49; found: 1378.51; elemental analysis calcd (%) for C₈₈H₇₄N₄O₈S₂: C 76.61, H 5.41, N 4.06, S 4.65; found: C 76.52, H 5.47, N 4.01, S 4.74.

Device fabrication

The fabrication process has been standardized in our group and optimized for CH₃NH₃PbI₃ as a sensitizer and spiro-OMeTAD as the HTM, under our laboratory conditions. The procedure is as follows: fluorine-doped tin oxide (FTO) glass was etched with zinc powder and a 2 M aqueous solution of HCl. A compact layer of TiO₂ was deposited onto the FTO surface by a spray pyrolysis process with a solution of titanium diisopropoxide bis(acetylacetonate) (75% in 2 propanol, Sigma-Aldrich) diluted in ethanol (1:9 v/v). After cooling to room temperature, the substrates were treated with a 0.04 M solution of TiCl₄ for 30 min at 70 °C. A mesoporous TiO₂ film was spin-coated onto the FTO surface by using 30 nm TiO₂ nanoparticle paste diluted with ethanol (1:5 w/w) and sintered at 500 °C for 30 min. The films were treated with a 40 mM solution of TiCl₄ at 70 °C for 30 min and heated at 500 °C again for 30 min. After cooling to RT, a 1 M solution of PbI₂ was spin-coated onto the mesoporous film, which was then heated at 70 °C for 30 min. The films were then immersed into a 8 mg mL⁻¹ solution of CH₃NH₃I in isopropanol (IPA) for 15 min, after which time they were rinsed with IPA and dried by spinning at 4000 rpm for 30 s, followed by annealing at 70 °C for 30 min. Spiro-OMeTAD (for the reference cell), H111, and H112 were each dissolved in chlorobenzene at a concentration of 100 mg mL⁻¹, with heating to 70 °C for 30 min. *tert*-Butylpyridine (TBP; 15.92 μL) and lithium bis(trifluoromethylsulfonyl)imide (Li-TFSI; 9.68 μL 520 mg mL⁻¹ in acetonitrile) were added directly to aliquots (300 μL) of the HTM solutions. Codopant tris[2-(1*H*-pyrazol-1-yl)pyridine]cobalt(III) tris(hexafluorophosphate) (FK102) was predissolved into acetonitrile and added to the solution of HTM at ratio of 15 mol %. The as-prepared solutions were spin-coated onto the film at 4000 rpm for 30 s. A 100 nm Au cathode layer was deposited by thermal evaporation through a 0.2 cm² metallic mask.

Equipment

¹H and ¹³C NMR data were obtained on a Bruker DPX 400 MHz spectrometer with chemical shifts referenced to CD₂Cl₂. CV measurements were carried out on a CHI411 electrochemical workstation, by using a concentration of a few mM in dichloromethane containing approximately 0.1 M of tetrabutylammonium hexafluorophosphate ([Bu₄N][PF₆]) supporting electrolyte, in a three-electrode cell, in which the Ag/AgCl electrode was used as the reference electrode and platinum wire as the working electrode. The scanning rate was 100 mV s⁻¹ and ferrocene was used for calibration. The absorption spectra were measured by using a SHIMADZU UV-3600 UV/Vis/near-infrared (NIR) spectrophotometer. DSC was run on a TA Instrument Q10. Photovoltaic measurements utilized an AM 1.5G solar simulator equipped with a 450 W xenon lamp (model 81172, Oriel). Its power output was adjusted to match AM 1.5G sunlight (100 mW cm⁻²) by using a reference Si photodiode. The *I*-*V* curves were obtained by applying an external bias to the cell and measuring the generated photocurrent with a Keithley model 2612A digital source meter. All devices were measured by masking the active area with a black tape mask. The IPCE was

measured by using a PVE300 (Bentham) instrument, with a dual xenon/quartz halogen light source, measured in direct current (DC) mode and no bias light was used. For the EIS study, measurements were carried out by using an AutoLab PGSTAT302N instrument under illumination conditions, and different bias potentials were applied ranging from 0.05 V to open-circuit voltage and frequencies between 1 MHz and 1 Hz.

Acknowledgements

Funding from the National Research Foundation (NRF), Singapore, is acknowledged (CRP Award No.: NRF-CRP4-2008-03).

Keywords: dyes/pigments • electrochemistry • heterocycles • perovskite phases • solar cells

- [1] B. O'Regan, M. Grätzel, *Nature* **1991**, *353*, 737–740.
- [2] S. Mathew, A. Yella, P. Gao, R. Humphry-Baker, B. F. E. Curchod, N. Ashari-Astani, I. Tavernelli, U. Rothlisberger, M. K. Nazeeruddin, M. Grätzel, *Nat. Chem.* **2014**, *6*, 242–247.
- [3] H. Sakamoto, S. Igarashi, M. Uchida, K. Niume, M. Nagai, *Org. Electron.* **2012**, *13*, 514–518.
- [4] I. Chung, B. Lee, J. He, R. P. H. Chang, M. G. Kanatzidis, *Nature* **2012**, *485*, 486–489.
- [5] P. Qin, S. Tanaka, S. Ito, N. Tetreault, K. Manabe, H. Nishino, M. K. Nazeeruddin, M. Grätzel, *Nat. Commun.* **2014**, *5*, 3834.
- [6] a) L. Yang, U. B. Cappel, E. L. Unger, M. Karlsson, K. M. Karlsson, E. Gabrielson, L. Sun, G. Boschloo, A. Hagfeldt, E. M. J. Johansson, *Phys. Chem. Chem. Phys.* **2012**, *14*, 779–789; b) J. Melas-Kyriazi, I. K. Ding, A. Marchioro, A. Punzi, B. E. Hardin, G. F. Burkhard, N. Tetreault, M. Grätzel, J.-E. Moser, M. D. McGehee, *Adv. Energy Mater.* **2011**, *1*, 407–414; c) U. B. Cappel, E. A. Gibson, A. Hagfeldt, G. Boschloo, *J. Phys. Chem. C* **2009**, *113*, 6275–6281; d) H. J. Snaith, R. Humphry-Baker, P. Chen, I. Cesar, S. M. Zakeeruddin, M. Grätzel, *Nanotechnology* **2008**, *19*, 424003; e) H. J. Snaith, M. Grätzel, *Adv. Mater.* **2007**, *19*, 3643–3647; f) H. J. Snaith, M. Grätzel, *Appl. Phys. Lett.* **2006**, *89*, 262114; g) J. Krüger, R. Plass, M. Grätzel, P. J. Cameron, L. M. Peter, *J. Phys. Chem. B* **2003**, *107*, 7536–7539; h) J. Krüger, R. Plass, L. Cevey, M. Piccirelli, M. Grätzel, U. Bach, *Appl. Phys. Lett.* **2001**, *79*, 2085–2087; i) U. Bach, Y. Tachibana, J.-E. Moser, S. A. Haque, J. R. Durrant, M. Grätzel, D. R. Klug, *J. Am. Chem. Soc.* **1999**, *121*, 7445–7446; j) U. Bach, D. Lupo, P. Comte, J. E. Moser, F. Weissörtel, J. Salbeck, H. Spreitzer, M. Grätzel, *Nature* **1998**, *395*, 583–585; k) M. M. Lee, J. Teuscher, T. Miyasaka, T. N. Murakami, H. J. Snaith, *Science* **2012**, *338*, 643–647.
- [7] a) A. Kojima, K. Teshima, Y. Shirai, T. Miyasaka, *J. Am. Chem. Soc.* **2009**, *131*, 6050–6051; b) J.-H. Im, C.-R. Lee, J.-W. Lee, S.-W. Park, N.-G. Park, *Nanoscale* **2011**, *3*, 4088–4093; c) L. Etgar, P. Gao, Z. Xue, Q. Peng, A. K. Chandiran, B. Liu, M. K. Nazeeruddin, M. Grätzel, *J. Am. Chem. Soc.* **2012**, *134*, 17396–17399; d) H.-S. Kim, C.-R. Lee, J.-H. Im, K.-B. Lee, T. Moehl, A. Marchioro, S.-J. Moon, R. Humphry-Baker, J.-H. Yum, J. E. Moser, M. Grätzel, N.-G. Park, *Sci. Rep.* **2012**, *2*, 591; e) J.-Y. Jeng, Y.-F. Chiang, M.-H. Lee, S.-R. Peng, T.-F. Guo, P. Chen, T.-C. Wen, *Adv. Mater.* **2013**, *25*, 3727–3732; f) J. H. Heo, S. H. Im, J. H. Noh, T. N. Mandal, C.-S. Lim, J. A. Chang, Y. H. Lee, H.-j. Kim, A. Sarkar, M. K. Nazeeruddin, M. Grätzel, S. I. Seok, *Nat. Photonics* **2013**, *7*, 486–491; g) M. J. Carnie, C. Charbonneau, M. L. Davies, J. Troughton, T. M. Watson, K. Wojciechowski, H. Snaith, D. A. Worsley, *Chem. Commun.* **2013**, *49*, 7893–7895; h) B. Cai, Y. Xing, Z. Yang, W.-H. Zhang, J. Qiu, *Energy Environ. Sci.* **2013**, *6*, 1480–1485.
- [8] a) M. Liu, M. B. Johnston, H. J. Snaith, *Nature* **2013**, *501*, 395–398; b) N. J. Jeon, H. G. Lee, Y. C. Kim, J. Seo, J. H. Noh, J. Lee, S. I. Seok, *J. Am. Chem. Soc.* **2014**, *136*, 7837–7840.
- [9] a) D. Bi, L. Yang, G. Boschloo, A. Hagfeldt, E. M. J. Johansson, *J. Phys. Chem. Lett.* **2013**, *4*, 1532–1536; b) E. Edri, S. Kirmayer, D. Cahen, G. Hodes, *J. Phys. Chem. Lett.* **2013**, *4*, 897–902.
- [10] N. J. Jeon, J. Lee, J. H. Noh, M. K. Nazeeruddin, M. Grätzel, S. I. Seok, *J. Am. Chem. Soc.* **2013**, *135*, 19087–19090.

- [11] H. Li, K. Fu, A. Hagfeldt, M. Grätzel, S. G. Mhaisalkar, A. C. Grimsdale, *Angew. Chem. Int. Ed.* **2014**, *53*, 4085–4088; *Angew. Chem.* **2014**, *126*, 4169–4172.
- [12] M. Takahashi, K. Masui, H. Sekiguchi, N. Kobayashi, A. Mori, M. Funahashi, N. Tamaoki, *J. Am. Chem. Soc.* **2006**, *128*, 10930–10933.
- [13] T. Leijtens, I. K. Ding, T. Giovenzana, J. T. Bloking, M. D. McGehee, A. Sellinger, *ACS Nano* **2012**, *6*, 1455–1462.
- [14] H. J. Snaith, *Adv. Funct. Mater.* **2010**, *20*, 13–19.
- [15] a) A. Dualeh, T. Moehl, N. Tétreault, J. Teuscher, P. Gao, M. K. Nazeeruddin, M. Grätzel, *ACS Nano* **2014**, *6*, 362–373; b) B. Suarez, V. Gonzalez-Pedro, T. S. Ripolles, R. S. Sanchez, L. Otero, I. Mora-Sero, *J. Phys. Chem. Lett.* **2014**, *5*, 1628–1635.
- [16] H.-S. Kim, J.-W. Lee, N. Yantara, P. P. Boix, S. A. Kulkarni, S. Mhaisalkar, M. Grätzel, N.-G. Park, *Nano Lett.* **2013**, *13*, 2412–2417.

Received: June 25, 2014Published online on September 18, 2014
